Contents lists available at ScienceDirect

European Journal of Radiology Open

Full Length Article

Differentiation of prostate cancer lesions in the Transition Zone by diffusion-weighted MRI

Jie Bao[a,1], Ximing Wang[a,1], Chunhong Hu[a,*], Jianquan Hou[b], Fenglin Dong[c], Lingchuan Guo[d]

[a] Department of Radiology, The First Affiliated Hospital of Soochow University, 188#, Shizi Road, Suzhou, 215006, China
[b] Department of Urology, The First Affiliated Hospital of Soochow University, Suzhou, 215000, China
[c] Department of Ultrasound, The First Affiliated Hospital of Soochow University, Suzhou, 215000, China
[d] Department of Pathology, The First Affiliated Hospital of Soochow University, Suzhou, 215000, China

ARTICLE INFO

ABSTRACT

Objective: To differentiate prostate cancer lesions in transition zone by diffusion-weighted-MRI (DW-MRI).
Methods: Data from a total of 63 patients who underwent preoperative DWI (b of 0–1000 s/mm^2) were prospectively collected and processed by a monoexponential (DWI) model and compared with a biexponential (IVIM) model for quantitation of apparent diffusion coefficients (ADCs), perfusion fraction f, diffusivity D and pseudo-diffusivity D*. Histogram analyses were performed by outlining entire-tumor regions of interest (ROIs). These parameters (separately and combined in a logistic regression model) were used to differentiate lesions depending on histopathological analysis of Magnetic Resonance/transrectal Ultrasound (MR/TRUS) fusion-guided biopsy. The diagnostic ability of differentiate the PCa from BHP in TZ was analyzed by ROC regression. Histogram analysis of quantitative parameters and Gleason score were assessed with Spearman correlation.
Results: Thirty (30 foci) cases of PCa in PZ and 33 (36 foci) cases of BPH were confirmed by pathology. Mean ADC, median ADC, 10th percentile ADC, 90th percentile ADC, kurtosis and skewness of ADC and mean D values, median D and 90th percentile D differed significantly between PCa and BHP in TZ. The highest classification accuracy was achieved by the mean ADC (0.841) and mean D (0.809). A logistic regression model based on mean ADC and mean D led to an AUC of 0.873, however, the difference is not significant. There were 7 Gleason 6 areas, 9 Gleason 7 areas, 8 Gleason 8 areas, 5 Gleason 9 areas and 2 Gleason 10 areas detected from the 31 prostate cancer areas, the mean Gleason value was(7.5 ± 1.2). The mean ADC and mean D had correlation with Gleason score(r = −0.522 and r = −0.407 respectively, P < 0.05).
Conclusion: The diagnosis efficiency of IVIM parameters was not superior to ADC in the diagnosis of PCa in TZ. Moreover, the combination of mean ADC and mean D did not perform better than the parameters alone significantly; It is feasible to stratify the pathological grade of prostate cancer by mean ADC.

1. Introduction

Since prostate cancer (PCa) has unfortunately become a common cancer in men in more economically-developed countries, it is significant to detect these lesions, especially in the transition zone (TZ) of prostate. It was reported that between 25% and 40% of these cancers were TZ cancers [1–3]. Because the TZ is commonly the site of origin of benign prostatic hyperplasia (BPH) [4,5], which has a heterogeneous appearance, it is difficult to differential diagnose these lesions.

Therefore, differentiation of PCa from BPH is always a major problem frequently missed during clinical evaluation.

T2-weighted magnetic resonance (MR) imaging has been used widely for the evaluation of prostate cancer but with limited sensitivity and specificity [6–8]. More advanced functional MR imaging sequences in a custom multiparametric MR imaging (mpMRI) exam have been shown to significantly improve the performance of MRI in cancer diagnosis [9]. In addition, DWI has become a useful tool for differentiating malignant and benign prostatic tissue due to high contrast

resolution and the quantitative apparent diffusion coefficient (ADC) [6,10]. DWI reflects and measures the diffusion of water molecules within biological tissues due to thermal Brownian motion. However, because the monoexponential ADC calculated from DWI potentially mixes the diffusion of molecular and the perfusion of microcirculation blood in the capillaries, the Intravoxel Incoherent Motion (IVIM) model may better account for the pseudo-diffusion based on microvascular perfusion from tissue diffusion [11]. In recent years, several studies examined prostate IVIM in the comparison of cancerous regions and normal tissue [12–14] without partition of the prostate, but the comparison of DWI and IVIM for tumor in TZ has not been reported at length. In addition, the traditional manually selected regions of interest (ROIs) has been pointed out as a limitation in many studies in which the overlap of a single measurement, which may lead to interobserver variability in ROI placement [15–17]. Histogram-based analysis has become to be a more objective approach the measure the diffusion-based parameters based on an entire-tumor region, and will be used here.

Therefore, the purpose of this study was to primarily assess the diagnostic performance of DWI (using a monoexponential fit for ADC) and IVIM (using a biexponential model) for the differential diagnosis of PCa in TZ on the basis of an entire-tumor histogram analysis, by using Magnetic Resonance/transrectal Ultrasound (MR/TRUS) targeted biopsy results as the reference (gold) standard.

2. Materials and methods

2.1. Patients

This prospectively designed, single institutional study was conducted in concordance with the standards of the local ethics committee. Forty-nine consecutive subjects were recruited and underwent mpMRI at 3T between January and December 2016 before biopsy. Inclusion criteria included (1) patient having undergone no prior hormonal or radiation treatment, (2) all the diffusion imaging studies having the same parameters, (3) the diameter of proven tumors being at least 0.5 cm in size, and (4) the tumor was considered as originated from a histological zone if more than 70% of its surface was located in TZ [18].

2.2. MR acquisition

MRI studies were carried out on a 3.0 T MR scanner (MAGNETOM Skyra, Siemens Healthcare, Erlangen, Germany) and a pelvic phased-array coil. As per the standard clinical prostate MR examination at our institution, the images obtained included transverse T1-weighted turbo spin-echo (TSE) images (repetition and echo times, 700/13 ms; flip angle, 120; section thickness, 3 mm; intersection gap, 0 mm; field of view, 320mm × 250 mm; and matrix, 384 × 336). Transverse, coronal, and sagittal T2-weighted TSE images (4000/89 ms; flip angle, 120; section thickness, 3 mm; intersection gap, 0 mm; field of view, 240mm × 240 mm; and matrix, 384 × 336) were also acquired. Finally, single-shot echo-planar imaging (6800/98 ms; flip angle, 90; field of view, 160mm × 296 mm; matrix, 192 × 130; section thickness, 3 mm; intersection gap, 0 mm; a parallel imaging factor of 2; and 13 sections) was performed with a Stejskal-Tanner diffusion module and added fat suppression pulses. Diffusion in three orthogonal directions was measured from b values of 0, 50, 100, 150, 200, 500, and 1000s/mm^2, for a total scan time of 5 min and 30 s.

2.3. Imaging and histological correlation(MR/TRUS fusion-guided biopsy)

All suspicious lesions from the MRI examination received MRI-TRUS fusion puncture within one week of the MR. All patients were anesthesized by intravenous injection and underwent transperineal prostate biopsy. In order to plan the biopsy puncture, DICOM data of mpMRI images were guided into RVS ultrasound host, selecting the

obvious and scored abnormal signal on T2WI, DWI or DCE images and marking the target lesions as ROI. Prostate sagittal scans of TRUS were used to match the ROI and the same section using urethra, prostate, ejaculatory duct cyst or cysts and other anatomical landmarks, then switched to the axial cross-section using seminal vesicle, bladder and other anatomical landmarks further to correct MRI-TRUS images synchronously. After confirming MRI-TRUS images and TRUS for prostate sagittal scan, the "+" target lesions were found in real-time. After marking each partition details, each specimen was fixed in 10% formalin and sent for a pathology puncture analysis.

2.4. Diffusion MRI post-processing

All images were transferred in Digital Imaging and Communications in Medicine DICOM format and post-processed offline with in-house software (FireVoxel; CAI2 R, New York University, NY) and MATLAB software (MathWorks Inc. Natick, MA, USA). The biexponential IVIM and monoexponential ADC measures were respectively post-processed.

The following biexponential (IVIM) equation was used:

$$S(b)/S0 = fe^{-bD*} + (1 - f)^{-bD}$$

Where S(b) is the mean signal intensity, S0 the signal reference, b is the b value and f is the perfusion fraction. D* is the diffusion of the perfusing fraction and D is the diffusion of the non-perfusing fraction.

The apparent diffusion coefficient (ADC) was computed on the same ROIs by linear regression from the isotropic images from each b-value according to the monoexponential equation:

$$S(b)/S0 = e^{-bADC}$$

In term of the histogram analyses, a voxel analysis of each independent tumor focus was performed, and the software (PASW Statistics 22.0; IBM,Corp, NY, USA) was used to calculate a histogram analysis. The following parameters were derived from the D, D*, f and ADC maps; ADC maps included the mean, median, 10th percentile, 90th percentile, and skewness. Given that the kurtosis is the degree of peakedness of a distribution, then skewness is a measure of the degree of asymmetry of a distribution. (the n th percentile is the point at which n% of the voxel values that form the histogram are found to the left).

2.5. Statistical analysis

All statistical analyses were performed by using SPSS 22.0 (IBM Corp, NY, USA) and Medcalc(15.0). P values of less than 0.05 determined statistical significance. Data satisfying the assumption (mean, median, the 10th and 90th percentiles) were subjected to independent sample t-test. Conversely, data not satisfying the assumption (kurtosis, skewness) were analyzed by using the Mann–Whitney U test. The parameters that yielded significance difference were selected for measuring the accuracy by using the area under the receiver operating characteristic (ROC) curve (Az). The other significance difference parameters were added to the top two Azs in logistic model by calculating Az by the method of Au Hoang Dinh[19]. The correlation of the parameters and Gleason score were assessed by Spearman correlation. All interval estimations provided in this article are 95% confidence intervals (CIs).

3. Results

Sixty-six patents were included in this study. Thirty (31 foci) cases of PCa in PZ with a mean age of 69 ± 1.54 years and a mean PSA level of 72.13 ± 26.93 ng/ml, and 30(33 foci) cases of BPH with a mean age of 63 ± 1.47 years and a mean PSA level of 12.90 ± 1.13 ng/ml were confirmed by pathology.

The results showed that PCa regions had significantly lower ADC values than the BHP regions in terms of histogram mean, median, 10th
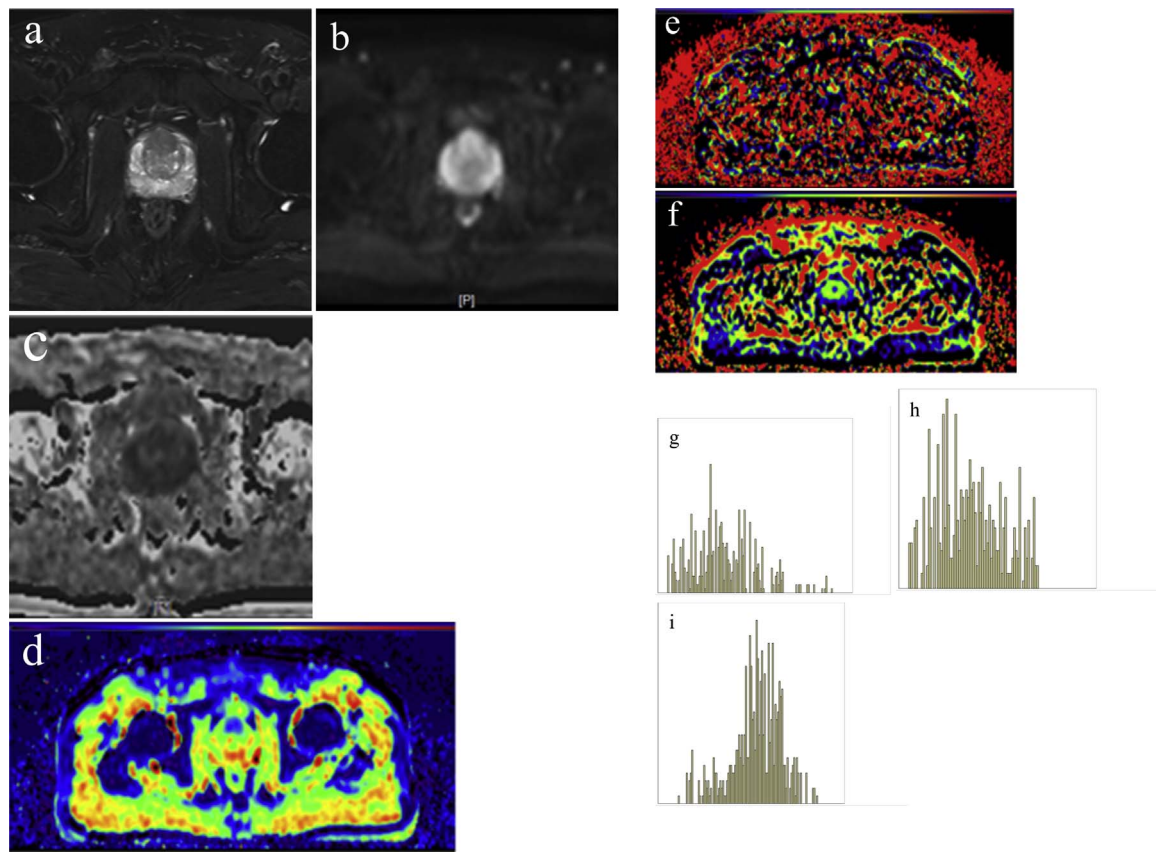
Fig. 1. A representative PCa for the histogram analysis of DW imaging measures, it shows a heterogeneous low signal intensity (SI) on T2-weighted images(a) and high SI on corresponding DW images(b, c) (b = 1000 s/mm²); The D (d), D* (e) and f(f) were obtained, respectively. The tumour boundary was then outlined and the pixel-by-pixel D (g), D* (h) and f (i) were obtained, and the corresponding histogram distributions were constructed, respectively.

Table 1
Histogram parameters of ADC and IVIM according to BHP and PCa.

Histogram analysis	BPH(n = 33)	PCa(n = 30)	P value
ADC(x10^{-3} mm²/s)			
Mean	1.59 ± 0.31	1.16 ± 0.28	< 0.001
Median	1.59 ± 0.53	1.14 ± 0.38	< 0.001
10th percentile	1.12 ± 0.21	0.92 ± 0.26	< 0.001
90th percentile	1.61 ± 0.41	0.94 ± 0.39	< 0.001
Skewness [M(P25,P75)]	0.0014 (0.0012,0.0014)	0.0013(0.0013,0.0095)	0.029
Kurtosis [M(P25,P75)]	0.147(−0.150,0.498)	−0.087 (-0.793, 0.898)	0.030
D(x10^{-3} mm²/s)			
Mean	1.44 ± 0.45	0.94 ± 0.39	< 0.001
Median	1.57 ± 0.79	1.14 ± 0.26	0.03
10th percentile	0.48 ± 0.39	0.46 ± 0.41	0.852
90th percentile	21.23 ± 8.4	19.16 ± 11.62	0.405
Skewness [M(P25,P75)]	1.26(0.81,1.62)	1.21(0.75,1.61)	0.761
Kurtosis [M(P25,P75)]	0.33 (−0.56,1.77)	0.46(−0.55,2.29)	0.919
D*(x10^{-3} mm²/s)			
Mean	14.43 ± 7.75	15.79 ± 6.88	0.453
Median	10.25 ± 9.85	11.56 ± 5.69	0.499
10th percentile	4.66 ± 2.80	3.64 ± 3.28	0.176
90th percentile	30.63 ± 20.85	29.12 ± 19.48	0.763
Skewness [M(P25,P75)]	3.09(2.23,4.13)	3.57(2.25,4.77)	0.259
Kurtosis [M(P25,P75)]	7.50(1.36,15.52)	11.17(3.38,22.09)	0.628
f(%)			
Mean	14.56 ± 1.00	14.97 ± 1.20	0.133
Median	18.61 ± 12.04	16.97 ± 4.56	0.478
10th percentile	6.22 ± 3.00	6.77 ± 3.10	0.464
90th percentile	18.57 ± 2.24	18.82 ± 0.49	0.541
Skewness [M(P25,P75)]	0.034(−0.691,0.513)	0.155(−0.234,0.603)	0.443
Kurtosis [M(P25,P75)]	−1.332(−1.760,−0.796)	−1.439(−1.6945,−0.841)	0.931

Data are means ± standard deviations; Data are medians with 25th percentile and 75th percentile in the parentheses. *Difference is significant; Numbers in the parentheses are the 95% Confidence Intervals (CIs).

Table 2

The effectiveness of histogram parameters in differentiating PCa from BHP in TZThe Az which closed to 0.5 were excluded; Numbers in the parentheses are 95% CIs.

Histogram analysis	Az (95% CI)	Sensitivity at threshold (%) (95% CI)	Specificity at threshold (%) (95% CI)	Youden index at threshold	PPV95%CI	NPV95%CI
ADC						
Mean	0.841(0.731 − 0.919)	87.10(70.2 − 96.4)	80.56 (64.0 − 91.8)	0.677	81.8(64.5 − 93.0)	88.2(72.5 − 96.7)
Median	0.766(0.647 − 0.861)	67.74 (48.6 − 83.3)	77.78(60.8 − 89.9)	0.455	72.4(52.8 − 87.3)	73.7(56.9 − 86.6)
10th percentile	0.729(0.606 − 0.830)	61.29(42.2 − 78.2)	83.33 (67.2 − 93.6)	0.446	76.0(54.9 − 90.6)	71.4(55.4 − 84.3)
90th percentile	0.747(0.626 − 0.845)	61.29(42.2 − 78.2)	80.56 (64.0 − 91.8)	0.419	73.1(52.2 − 88.4)	70.7(54.5 − 83.9)
D						
Mean	0.809(0.695 − 0.895)	70.97(52.0 − 85.8)	77.78 (60.8 − 89.9)	0.488	73.3(54.1 − 87.7)	75.7(58.8 − 88.2)
Median	0.715(0.592 − 0.819)	100.00(88.8 − 100.0)	44.44(27.9 − 61.9)	0.444	60.8(46.1 − 74.2)	100.0(79.4 − 100.0)
mean ADC+ mean D[*]	0.873(0.769 − 0.942)	87.10 (70.2 − 96.4)	83.33(67.2 − 93.6)	0.7043	81.8(64.5 − 93.0)	88.2(72.5 − 96.7)

* P = 0.346.

percentile, 90th percentile skewness and kurtosis (all p < 0.005) (Fig. 1). For the IVIM-derived D, the histogram mean, median, and the 90th percentile reflected statistically significant differences between PCa and BHP groups (all p < 0.005). For D* and f, the mean, median and 10th and 90th percentiles for D* and f differences were not significant between the two groups (all p > 0.05). All more details were showed in Table 1.

Table 2 displays the results of the ROC analysis of histogram parameters that had significance difference between PCa and BHP; the Az values which were close to 0.5 were excluded. The mean ADC (0.841) and mean D (0.809) had higher Az than other histogram parameters (Fig. 2a). In Table 3, histogram parameters of D values did not add significant independent information to the ADC (p > 0.05) (Fig. 2b). The correlation of the parameters and Gleason score is showed in Table 3.

4. Discussion

This is the first published study to evaluate more detailed information noninvasively through histogram analyses of PCa from BPH using monoexponential (DWI) and biexponential (IVIM) models. The results demonstrate that PCa and BHP in TZ can be differentially diagnosed by multiparametric ADC and IVIM MR imaging with histogram analysis. We first compared the ADC and IVIM histogram parameters obtained from the PCa and BPH in TZ in order to evaluate if there are any significant differences. All of the ADC histogram parameters, mean, median and 90th percentile D were significantly lower in PCa than BPH, indicating more heterogeneity and complexity of cellularity in a tumor region than in BPH. However, the histogram D* and f had no statistic significance difference, which means pseudo-perfusion may contribute little to the diffusivity for detecting PCa in TZ. Conversely, in our results, spearman coefficient analysis revealed significant negative correlations between Gleason score and mean ADC and mean D, the statistic difference is significant, in the similar finding Yang [20] reported that Gleason score was also negative correlations with ADC and D. However, some studies [21,12] found that decreased perfusion fraction may be involved in reducing ADC in prostate cancer. Thus, the relationship between diffusion parameters and Gleason remains controversial.

DWI is currently considered an important component of prostate mpMRI examinations, where it has been established as an important sequence for the detection of PCa [14]. However, as a possible improvement of DWI, it might be necessary to evaluate separately the two components of diffusion: the pure molecular diffusion and the perfusion-related diffusion (pseudo-diffusion) originating from capillary microcirculation. IVIM, by applying a biexponential model, allows the extraction of pure molecular diffusion parameters (D) and perfusion-related diffusion parameters (D* and f), as theorized.

In recent years, several studies have considered the relationship of IVIM with the PCa and BHP. Dopfert, J. [21] reported that the ADC, D
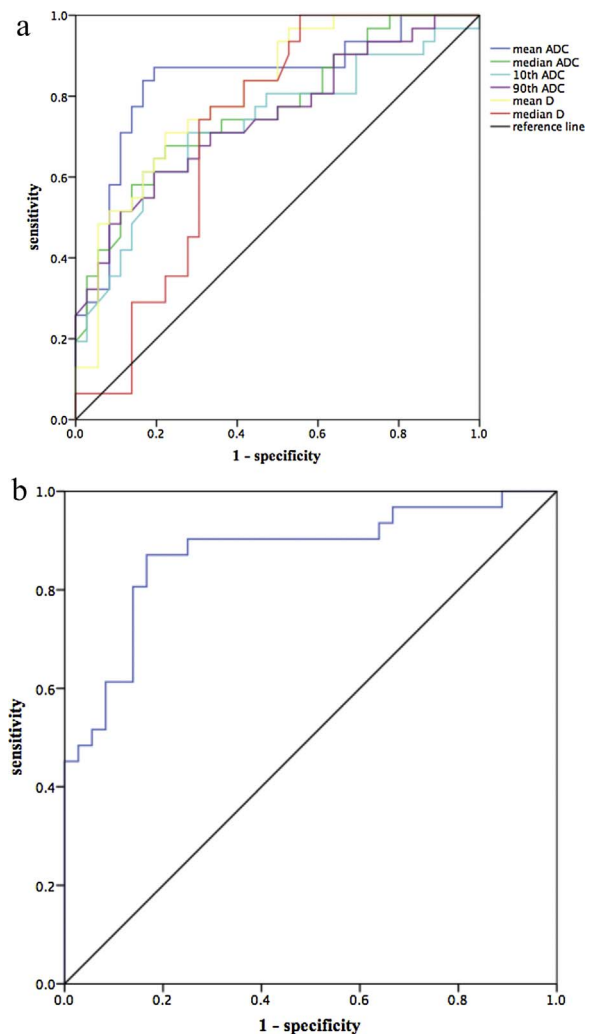

Fig. 2. Receiver Operating Characteristic (ROC) curves which illustrate the performance of the statistically significant difference parameters when distinguishing between PCa and BHP in TZ(a); ROC curves of combination of parameters based on mean ADC and mean D (b).

and f were significantly lowered in cancerous tissue to benign tissue; however, in the study of Shinmoto, H [13], f of prostate cancer and BPH were not significantly different. The results of those studies were inconsistent. In this study, we found that both ADC and D were excellent for detecting PCa from BHP. The idea is that in prostatic carcinoma, those parameters were clearly influenced by the amount of space available for extracellular water but was also dependent on the structural nature of this space [22], and the acinar structures were replaced

Table 3
The correlation between the parameters and Gleason score.

	ADC	D
mean	− 0.522[a]	− 0.407[a]
mean	− 0.218	− 0.093
10th percentile	− 0.167	/
90th percentile	− 0.286	/

[a] The difference is significant;/none.

by the more tightly packed cancer cells.

The D* and f calculated with the biexponential model had very large associated standard deviations, possibly reflecting physiologically based variability. The growth of prostate cancer is associated with the development of a rich blood supply fed by a large network of immature, leaky blood vessels [23], which is why the vascular perfusion made little contribution to DWI signal in the PCa. Although their clinical value may be limited, this further demonstrates the need for this highly variable perfusion component to be excluded to increase the clinical utility of the diffusion coefficient in diagnosis, prognosis or treatment response [24].

In this study, we first tried to combine traditional ADC with IVIM parameters, and found that the histogram of D was able to distinguish PCa from BHP in TZ, which was second to the mean ADC. In addition, median, 10th percentile, 90th percentile ADC and median D did not reflect statistical significance differences between inter-groups, had higher Az values than the kurtosis and skewness of ADC, the obtained Az for histogram skewness and kurtosis did not arrive at statistical significance by a linear regression model test. Unfortunately a logistic regression model combining the histogram parameters of ADC and D did not perform significantly better in detecting cancer in TZ than ADC alone. Therefore, our study suggests that the histogram of ADC and D provide the same information when discriminating between PCa and BHP in TZ compared with simple measurements of the mean values of these parameters. However, the lack of significant differences between the histogram of ADC and IVIM suggests that the measuring the histogram of ADC and D may not provide any additional information when discriminating between PCa and BHP in TZ.Therefore, our study suggests that measuring the histogram percentiles of ADC and IVIM values may not provide any additional information when discriminating PCa from BPH compared with simple measurements of the mean values of these parameters.

Recently, the literature has shown that the MR/TRUS fusion-biopsy system is increasingly being used to estimate the diagnostic performance of the PI-RADS scoring system in PCa. [25,26,9]. MR/TRUS fusion-biopsy is routinely used in clinical practice to integrate into biopsy planning information gained by MRI [27]. MRI-TRUS fusion biopsy has been reported to display a high rate of detection of clinically significant PCa with traditional TRUS biopsy [28,27,29]. Currently, TRUS biopsy of the prostate represents the gold standard for diagnosis of PCa before surgery; however, the rate of false-negative results can be as high as 35%, depending on the biopsy findings. In addition, the sensitivity and specificity for the detection of malignant lesions are limited. In contrast to traditional TRUS-guided biopsy, MRI-TRUS fusion biopsy effectively avoids the shortcomings of traditional biopsy, using the flexibility of ultrasound biopsy and electronically superimposing this on TRUS images in real time. Moreover, this study used transperineal MR/TRUS fusion biopsy. The advantages of a transperineal approach compared to a transrectal one includes reduced susceptibility to compression and mobilization of the prostate [9].

The study has a few limitations. First, there was no comparison of diagnostic efficacy located for different areas of the prostate, the future research should be allowed for a more comparable differentiation between the PCa in PZ and TZ; Second, larger patient populations would be needed to find the true correlation of histogram parameters and

aggressiveness and pathological grade of the tumor. Although the patients in this study were comparable to similar studies, it is still insufficient to analyze additional potential predictor variables.

In conclusion, our study found that mean ADC values differed between PCa and BHP in TZ. In addition, diffusivity mean D derived from IVIM could be a useful tool for discriminating PCa from BPH in TZ, However, information provided by IVIM did not lead to more improved classification results of PCa and BHP than ADC.

Conflicts of interest

The authors have no conflicts of interest to declare.

Funding

Acknowledgements

References

[1] J. Davis, W.J. Kim, J.F. Ward, et al., Radical prostatectomy findings in patients predicted to have low-volume/low-grade prostate cancer diagnosed by extended-core biopsies: an analysis of volume and zonal distribution of tumour foci, BJU Int. 105 (10) (2010) 1386–1391.

[2] V. Patel, G.S. Merrick, Z.A. Allen, et al., The incidence of transition zone prostate cancer diagnosed by transperineal template-guided mapping biopsy: implications for treatment planning, Urology 77 (5) (2011) 1148–1152.

[3] C. Siegel, Re Transition zone prostate cancer: detection and localization with 3-T multiparametric MR imaging, J. Urol. 190 (3) (2013) 881.

[4] J. McNeal, J. Noldus, Limitations of transition zone needle biopsy findings in the prediction of transition zone cancer and tissue composition of benign nodular hyperplasia, Urology 48 (5) (1996) 751–756.

[5] A. Reissigl, J. Pointner, H. Strasser, et al., Frequency and clinical significance of transition zone cancer in prostate cancer screening, Prostate 30 (2) (1997) 130–135.

[6] K.W. Doo, D.J. Sung, B.J. Park, et al., Detectability of low and intermediate or high risk prostate cancer with combined T2-weighted and diffusion-weighted MRI, Eur. Radiol. 22 (8) (2012) 1812–1819.

[7] L.M. Wu, J.R. Xu, Y.Q. Ye, et al., The clinical value of diffusion-weighted imaging in combination with T2-weighted imaging in diagnosing prostate carcinoma: a systematic review and meta-analysis, AJR Am. J. Roentgenol. 199 (1) (2012) 103–110.

[8] X. Wang, J.Y. Wang, C.M. Li, et al., Evaluation of the prostate imaging reporting and data system for magnetic resonance imaging diagnosis of prostate cancer in patients with prostate-specific antigen < 20 ng/ml, Chin. Med. J. (Engl.) 129 (12) (2016) 1432–1438.

[9] M.C. Roethke, T.H. Kuru, S. Schultze, et al., Evaluation of the ESUR PI-RADS scoring system for multiparametric MRI of the prostate with targeted MR/TRUS fusion-guided biopsy at 3.0 Tesla, Eur. Radiol. 24 (2) (2014) 344–352.

[10] L. Li, L. Wang, M. Deng, et al., Feasibility study of 3-T DWI of the prostate: readout-segmented versus single-shot echo-planar imaging, AJR Am. J. Roentgenol. 205 (1) (2015) 70–76.

[11] D. Le Bihan, E. Breton, D. Lallemand, et al., Separation of diffusion and perfusion in intravoxel incoherent motion MR imaging, Radiology 168 (2) (1988) 497–505.

[12] H. Shinmoto, C. Tamura, S. Soga, et al., An intravoxel incoherent motion diffusion-weighted imaging study of prostate cancer, AJR Am. J. Roentgenol. 199 (4) (2012) W496–500.

[13] T.H. Kuru, M.C. Roethke, B. Stieltjes, et al., Intravoxel incoherent motion (IVIM)

diffusion imaging in prostate cancer − what does it add? J. Comput. Assist. Tomogr. 38 (4) (2014) 558–564.

[14] M. Valerio, C. Zini, D. Fierro, et al., 3 T multiparametric MRI of the prostate: does intravoxel incoherent motion diffusion imaging have a role in the detection and stratification of prostate cancer in the peripheral zone? Eur. J. Radiol. 85 (4) (2016) 790–794.

[15] A.B. Rosenkrantz, B.E. Niver, E.F. Fitzgerald, et al., Utility of the apparent diffusion coefficient for distinguishing clear cell renal cell carcinoma of low and high nuclear grade, AJR Am. J. Roentgenol. 195 (5) (2010) W344–51.

[16] H. Wang, L. Cheng, X. Zhang, et al., Renal cell carcinoma: diffusion-weighted MR imaging for subtype differentiation at 3.0 T, Radiology 257 (1) (2010) 135–143.

[17] Y.D. Zhang, Q. Wang, C.J. Wu, et al., The histogram analysis of diffusion-weighted intravoxel incoherent motion (IVIM) imaging for differentiating the gleason grade of prostate cancer, Eur. Radiol. 25 (4) (2015) 994–1004.

[18] S. Bouye, E. Potiron, P. Puech, et al., Transition zone and anterior stromal prostate cancers: zone of origin and intraprostatic patterns of spread at histopathology, Prostate 69 (1) (2009) 105–113.

[19] A. Hoang Dinh, C. Melodelima, R. Souchon, et al., Quantitative analysis of prostate multiparametric MR images for detection of aggressive prostate cancer in the peripheral zone: a multiple imager study, Radiology 280 (1) (2016) 117–127.

[20] D.M. Yang, H.C. Kim, S.W. Kim, et al., Prostate cancer: correlation of intravoxel incoherent motion MR parameters with Gleason score, Clin. Imaging 40 (3) (2016) 445–450.

[21] J. Dopfert, A. Lemke, A. Weidner, et al., Investigation of prostate cancer using diffusion-weighted intravoxel incoherent motion imaging, Magn. Reson. Imaging 29 (8) (2011) 1053–1058.

[22] P. Gibbs, G.P. Liney, M.D. Pickles, et al., Correlation of ADC and T2 measurements with cell density in prostate cancer at 3.0 Tesla, Invest. Radiol. 44 (9) (2009) 572–576.

[23] D. Buckley, L.C. Roberts, G.J. Parker, et al., Prostate cancer: evaluation of vascular characteristics with dynamic contrast-enhanced T1-weighted MR imaging–initial experience, Radiology 233 (3) (2004) 709–715.

[24] S.F. Riches, K. Hawtin, E.M. Charles-Edwards, et al., Diffusion-weighted imaging of the prostate and rectal wall: comparison of biexponential and monoexponential modelled diffusion and associated perfusion coefficients, NMR Biomed. 22 (3) (2009) 318–325.

[25] E.M. Lawrence, S.Y. Tang, T. Barrett, et al., Prostate cancer: performance characteristics of combined T(2)W and DW-MRI scoring in the setting of template transperineal re-biopsy using MR-TRUS fusion, Eur. Radiol. 24 (7) (2014) 1497–1505.

[26] A.R. Rastinehad, N. Waingankar, B.et al Turkbey, Comparison of multiparametric MRI scoring systems and the impact on cancer detection in patients undergoing MR US fusion guided prostate biopsies, PLoS One 10 (11) (2015) e0143404.

[27] M. Roethke, A.G. Anastasiadis, M. Lichy, et al., MRI-guided prostate biopsy detects clinically significant cancer: analysis of a cohort of 100 patients after previous negative TRUS biopsy, World J. Urol. 30 (2) (2012) 213–218.

[28] S. Xu, J. Kruecker, B. Turkbey, et al., Real-time MRI-TRUS fusion for guidance of targeted prostate biopsies, Comput. Aided Surg. 13 (5) (2008) 255–264.

[29] P.A. Pinto, P.H. Chung, A.R. Rastinehad, et al., Magnetic resonance imaging/ultrasound fusion guided prostate biopsy improves cancer detection following transrectal ultrasound biopsy and correlates with multiparametric magnetic resonance imaging, J. Urol. 186 (4) (2011) 1281–1285.